Delft University of Technology

Computational Fluid Dynamics II Assignment

Delft University of Technology, Delft, South Holland, 2628 CD

Changkyu Park 4646061
Malte Wegener 4672194

Submission Date: February 8, 2021
Course: AE4136 (2020-2021)

Contents

1. Introduction

In this report, the Navier-Stokes solver is set up on a unit square using incidence and Hodge matrices. The solver is then validated using the given reference literature which presents the results produced by Botella and Peyret. The system of Navier-Stokes equations can be presented as

$$\frac{\partial u}{\partial t} - u \times \xi + \nabla P + \frac{1}{Re} \nabla \times \xi = 0 \,, \tag{1}$$

$$\nabla \cdot u = 0 \tag{2}$$

and

$$\xi = \nabla \times u \,, \tag{3}$$

where (1) and (2) represent the conservation of momentum and mass respectively. In these equations, u is the velocity flux, ξ represents vorticity which is found via (3), P equals $p + 1/2 \cdot |u|^2$ in which p is the pressure. Lastly, Re represents the Reynolds number.

To solve the system of equations, the vector operations

$$\text{grad} \equiv \nabla \,, \tag{4}$$

$$\text{curl} \equiv \nabla \times \tag{5}$$

and

$$\text{div} \equiv \nabla \cdot \tag{6}$$

are represented by incidence matrices, $\tilde{\mathbb{E}}$ for operations in primal grid (with tilde above letter) or $\mathbb{E}$ for operations in dual grid as presented in Figure 1. Since operations such as curl of vorticity as shown in (1) and conservation of mass in (2) are best done on primal grid while others like curl of velocity flux for the vorticity-velocity relation shown in (3) are best represented on dual grid, Hodge matrices $\mathbb{H}$ are also required to transfer the variables back and forth from dual grid to primal grid and vice versa which is also shown in Figure 1 where the Hodge matrices act as links between the two orientations.

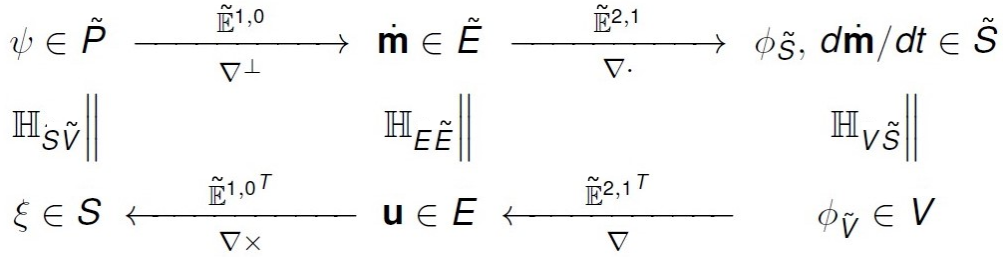

Fig. 1 Double DeRham sequence, adapted from [1]

Figure 1 features the double DeRham sequence that the numerical system of the report is based on. P represents points, E represents edges, S represents surfaces which in this report will be indicated as volumes and V represents vertices which will be indicated as points on dual grid in the report. ψ is the stream function, $\dot{m}$ is the mass flow across an edge on primal grid, ϕ is the velocity potential, ξ is the vorticity and u is the velocity flux along a dual edge.

2. Setup of the numerical system

To build the numerical system of the Navier-Stokes solver, multiple components such as the different incidence and Hodge matrices need to be created. Before setting up these matrices, the positive directions of the various variables on both primal and dual grids need to be defined. Additionally, the numbering for points, edges and volumes on these grids have to be defined to determine the values of elements in the matrices.

2.1. Defining positive directions and numbering system

Firstly, the (3×3) primal grid and its numbering system have been produced as an example as shown in Figure 2. An edge is added on each outer boundary and they contain prescribed values. The positive directions for the rotation around points, flux across edges, directionality of volumes have also been defined and presented with the red arrows.

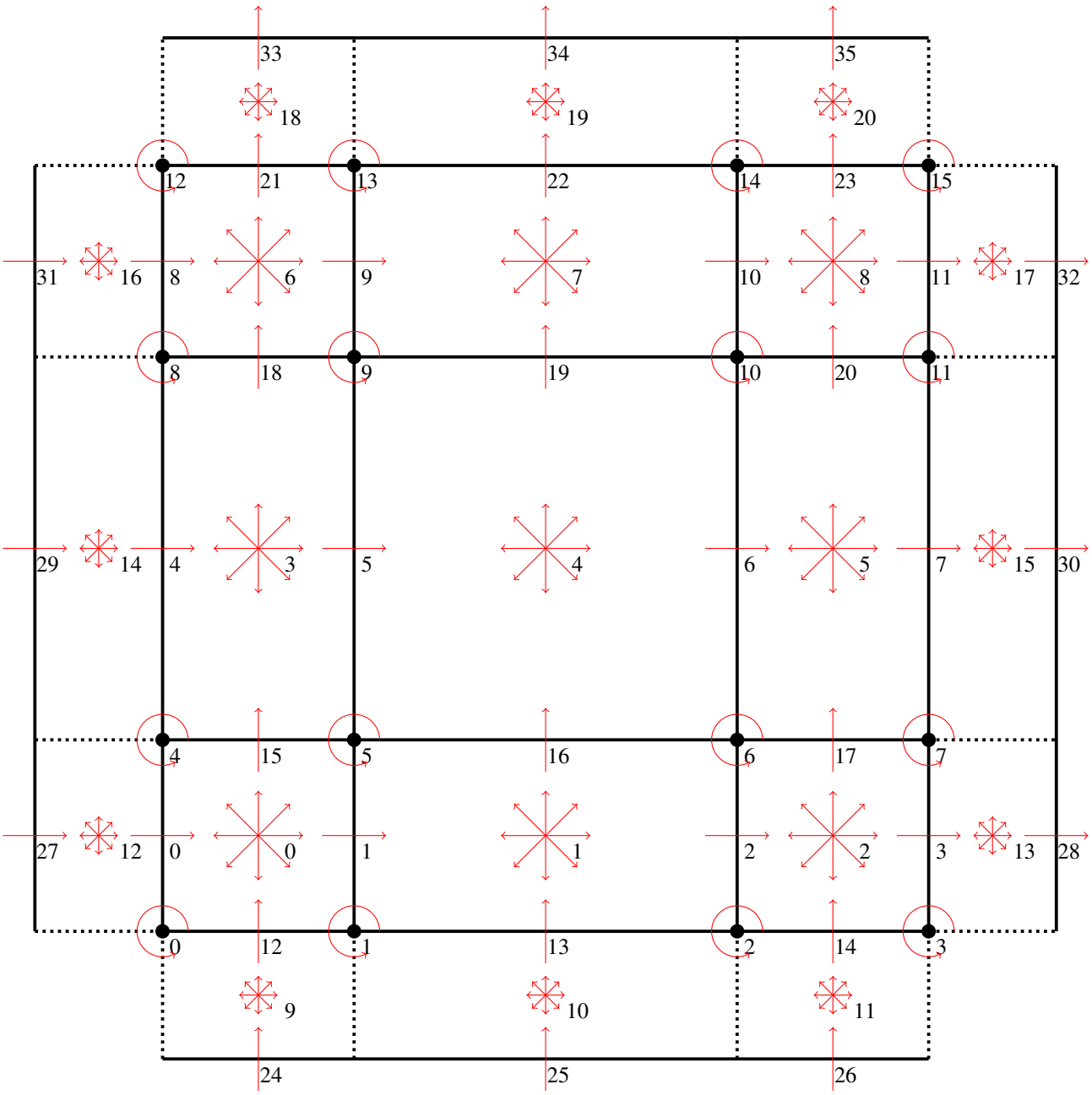

Fig. 2 Orientation of the primal grid and the numbering of its elements

2.2. Setup of incidence matrices

The divergence operator in the conservation of mass equation shown in (2) can be replaced with the incidence matrix and it reads

$$\tilde{\mathbb{E}}^{21}\tilde{u} = 0\,, \tag{7}$$

where $\tilde{u}$ represents velocity flux defined on primal grid and $\tilde{\mathbb{E}}^{21}$ represents the incidence matrix that relates edge (1) to volume (2) on the primal grid. For a (3×3) primal grid, this particular incidence matrix has a size of $(N^2 + 4N, 2N(N + 1)) = (21, 24)$ whereby the number of rows represents the number of volumes and the number of columns represents the number of velocity fluxes. The additional $4N$ number of volumes come from the additional edge present on each of the outer boundary. The full matrix is then visualised in Figure 3.

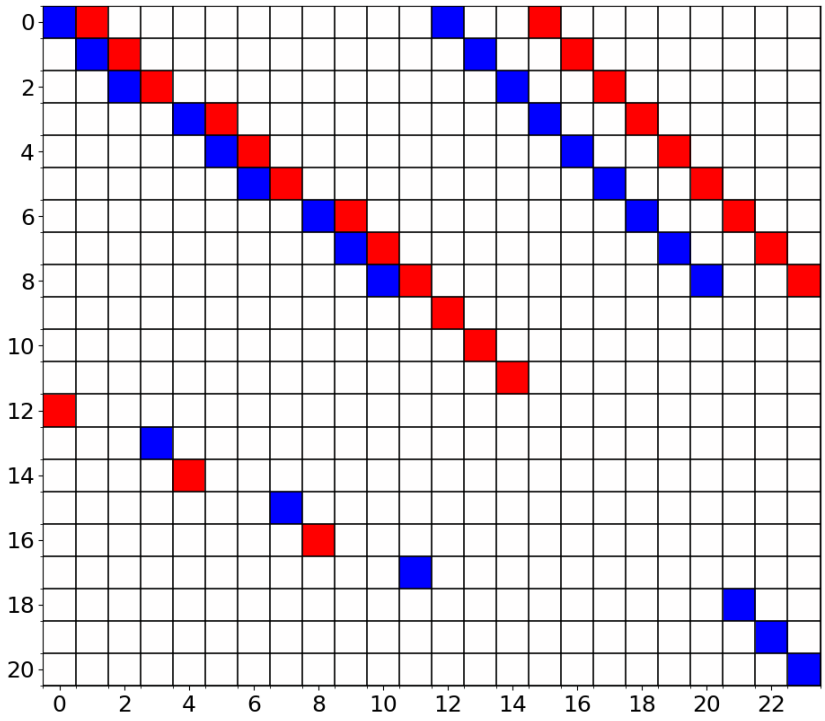

Fig. 3 Incidence matrix $\tilde{\mathbb{E}}^{21}$; red $= 1$, blue $= -1$

The $y-$axis of the matrix represents volumes and $x-$axis represents the edges. It is observed that $\tilde{\mathbb{E}}^{21}$ is of sparse nature with majority of its elements having 0 value. There exist four staggered diagonals for the inner volumes which have either a value of -1 or 1 which is determined by the agreement between the direction of velocity flux over the edge and its corresponding volume. From row 9 until 20 represent the link between volumes of outer boundary and the edges that they share with the inner volumes. These too have a value of either -1 or 1.

Since $\tilde{\mathbb{E}}^{21}$ features the last $4N$ number of rows representing the boundary volumes, the boundary conditions can be prescribed. They are implemented by introducing a vector with a length of $(N^2 + 4N)$ on the right-hand side of (7). The first N^2 elements of this vector are assigned a value of 0 since they correspond to the inner volumes and these receive no direct input from the boundary edges. The last $4N$ elements which correspond to the outer boundary volumes are then assigned values corresponding to the contributions from their respective outer boundary edges.

To discretize the Navier-Stokes equations, a dual grid has to be defined as well. This dual grid is shown in Figure 4. Every internal volume of the primal grid has an associated point in the dual grid, which is numbered according to the associated volume. This one-to-one mapping of the numbering is present for all elements of the dual grid. Furthermore, the inner orientation of dual surfaces and dual edges is the same as the outer orientation of its associated primal grid element. In contrast to this, the dual points are defined as sinks, opposite to the primal volumes, which are defined as sources.

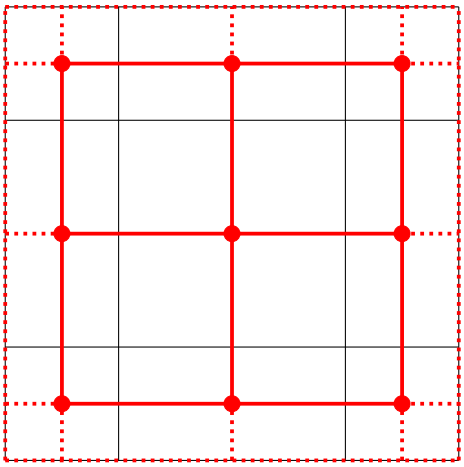

Fig. 4 Dual grid inside the primal grid

Since pressure P presented in (1) is defined on the dual grid, the incidence matrix which represents gradient on the dual grid needs to be set up. This incidence matrix $\mathbb{E}^{10}$ links the points to edges on dual grid and it has a size of $(2N(N+1), N^2+4N)$ whereby the number of rows corresponds to the number of edges and the number of columns corresponds to the number of points. It is to be noted that due to the $4N$ extra volumes on the outer boundary for the primal grid, there also are $4N$ extra points for the dual grid, thus extending the number of columns. This incidence matrix is set up similarly to $\tilde{\mathbb{E}}^{21}$, by assigning 1 or -1 depending on the agreement between the defined directions of fluxes along edges and sinks at points and taking the prescribed boundary conditions out of the matrix. $\mathbb{E}^{10}$ for $N = 3$ which has a size of $(24, 21)$ is visualised in Figure 5.

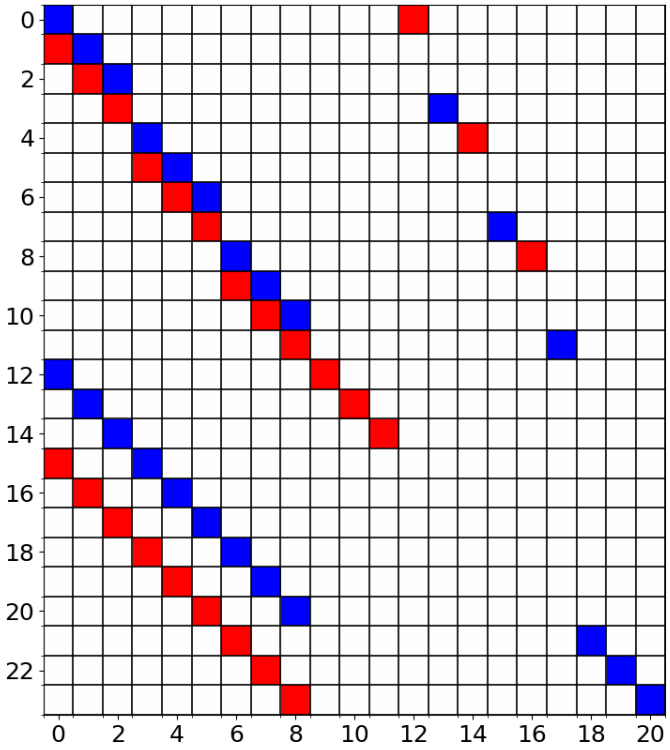

Fig. 5 Incidence matrix $\mathbb{E}^{10}$; red $= 1$, blue $= -1$

It can be clearly observed that $\mathbb{E}^{10}$ shown in Figure 5 is exactly a transpose of $\tilde{\mathbb{E}}^{21}$ shown in Figure 3.

Since the velocity fluxes are predefined on dual grid and that vorticity-velocity relation is to be solved on the dual grid, to solve (3), another incidence matrix $\mathbb{E}^{21}$ is required. This incidence matrix allows for computing

$$\xi^{(2)} = \mathbb{E}^{21} u^{(1)} \,, \tag{8}$$

which is conducted on the dual grid. $u^{(1)}$ represents the velocity fluxes along the edges of dual grid and $\xi^{(2)}$ represents the integrated vorticity in the volumes of the dual grid. Similarly to velocity flux across edges on primal grid, $u^{(1)}$, the velocity fluxes along the outer boundary edges are known and can be taken out from the equation. In doing so, (8) can be expressed as

$$\xi^{(2)} = \mathbb{E}^{21} u^{(1)} + u_{\text{prescr}} \tag{9}$$

whereby u_{prescr} represents the prescribed velocity fluxes along the edges of the outer boundary of the dual grid.

The incidence matrix $\mathbb{E}^{21}$ links the edges and volumes that exist on the dual grid as shown in Figure 4. This matrix has a size of $((N+1)^2, 2N(N+1))$. The number of rows represents the number of points and the number of columns represents the number of edges on the dual grid. Thus, for $N = 3$, the matrix has a size of $(16, 24)$ and this is also visualised in Figure 6.

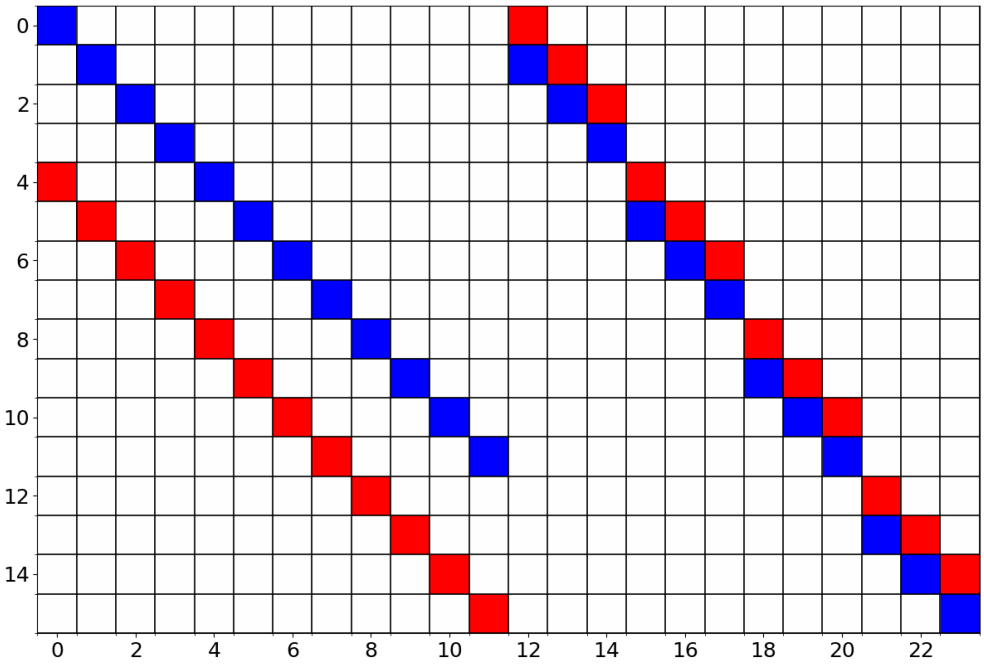

Fig. 6 Incidence matrix $\mathbb{E}^{21}$; red = 1, blue = −1

Similarly to the transpose relation between $\tilde{\mathbb{E}}^{21}$ and $\mathbb{E}^{10}$, the transpose of $\mathbb{E}^{21}$ shown in Figure 6 equals to $\tilde{\mathbb{E}}^{10}$ which is eventually required to be applied as curl in (1) which can be expressed as

$$\nabla \times \xi = \nabla \times (\nabla \times u) \tag{10}$$

which can be expressed in terms of incidence and Hodge matrices as

$$\nabla \times (\nabla \times u) = \mathbb{H}^{1\tilde{1}} \widetilde{\mathbb{E}}^{10} \mathbb{H}^{\widetilde{02}} \mathbb{E}^{21} u \tag{11}$$

in which the Hodge matrices $\mathbb{H}$ are introduced in the next section.

2.3. Hodge matrices

As aforementioned in Introduction, different operations are best done on different grid. Thus, in order to complete a set of operations, it is necessary to translate the involved variables from one grid to another and this is done via Hodge matrices $\mathbb{H}$ as shown in Figure 1.

Starting with $\mathbb{H}^{\tilde{1}1}$, this Hodge matrix translates the velocity fluxes along edges of dual grid $u^{(1)}$ to velocity fluxes across edges of primal grid $\tilde{u}^{(1)}$. These two velocity fluxes are defined as

$$\tilde{u}^{(1)} = \int_{\tilde{E}} \mathbf{u} \cdot \mathbf{n} \, \mathrm{d}l \tag{12}$$

and

$$u^{(1)} = \int_{E} \mathbf{u} \cdot \mathrm{d}\mathbf{l} \tag{13}$$

respectively where $\mathbf{u}$ represents velocity. Assuming constant velocity along the edges in the primal and dual grid, as well as orthogonality of the elements, this can be simplified to

$$\tilde{u}^{(1)} = |\tilde{h}| \mathbf{u} \cdot \mathbf{n} \tag{14}$$

$$u^{(1)} = |h| \mathbf{u} \cdot \mathbf{l} \tag{15}$$

As the edges on the dual and primal grid are oriented in the same direction, the transformation from dual to primal grid can be written as

$$\tilde{u}^{(1)} = \frac{|\tilde{h}|}{|h|} u^{(1)} \, , \tag{16}$$

where $\tilde{h}$ is the length of the edge on the primal grid for that specific velocity flux and h is the length of the edge on the dual grid for that specific velocity flux that is being translated. Similarly, $\mathbb{H}^{1\tilde{1}}$ is done by

$$u^{(2)} = \frac{|h|}{|\tilde{h}|} \tilde{u}^{(2)} \, . \tag{17}$$

Since the matrices involve translation of one specific velocity flux just one other velocity flux, they are square matrices. More specifically, they are of size $(2N(N+1), 2N(N+1))$. Furthermore, they are of diagonal matrices as shown in Figure 7 for an example of $N = 3$.

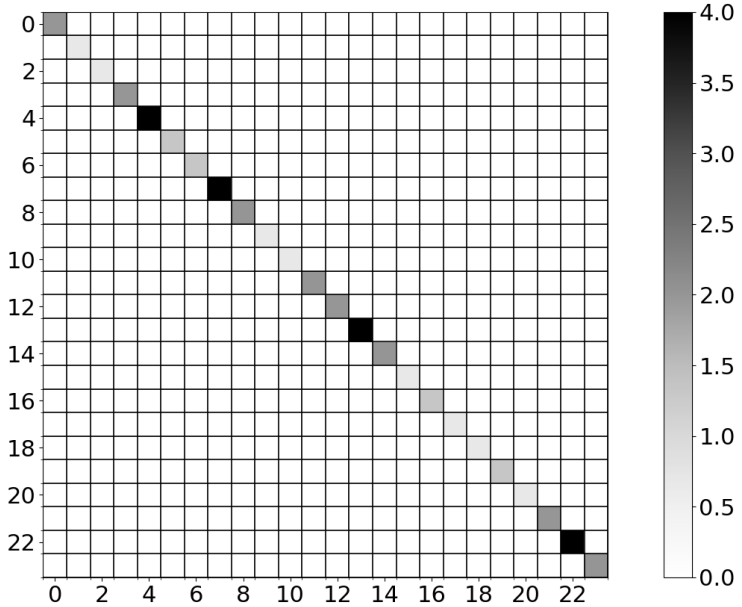

Fig. 7 Hodge matrix $\mathbb{H}^{\tilde{1}1}$

This diagonality can also be observed for $\mathbb{H}^{\tilde{0}2}$ which translates circulation $\xi^{(2)}$, defined as

$$\xi^{(2)} = \int_S \xi^{(0)} \, \mathrm{d}A \, , \tag{18}$$

on dual grid to vorticity on primal grid. However, unlike $\mathbb{H}^{\tilde{1}1}$ where it was an edge-to-edge translation that involves scaling of corresponding edge length, $\mathbb{H}^{\tilde{0}2}$ involves volumes that have areas (for this 2-dimensional case) and points that is of 0-dimension. For this transformation it is assumed that the vorticity distribution on the dual volume is constant over the dual volume. Thus, the translation is done by

$$\xi^{(0)} = \frac{1}{A} \xi^{(2)} \, , \tag{19}$$

where A is the corresponding area of the dual volume given by

$$A = h_x h_y \, , \tag{20}$$

in which h_x and h_y are the lengths of the relevant horizontal edge and vertical edge respectively. Again, since the number of points on primal grid matches the number of volumes on dual mesh and each point of primal grid corresponds to only one volume of dual grid and vice versa, the resultant matrix is a square matrix of size $((N+1)^2, (N+1)^2)$. Diagonality arises from the assumptions of constant vorticity distribution made for $\mathbb{H}^{\tilde{0}2}$. This Hodge matrix for $N = 3$ is also visualised as shown in Figure 8.

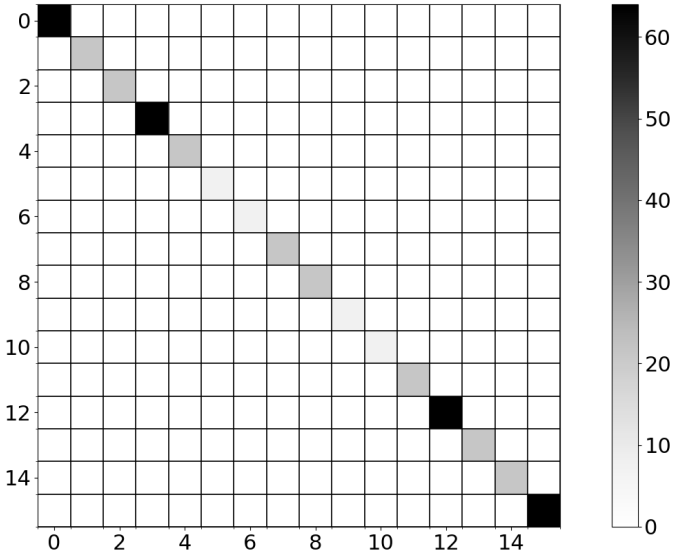

Fig. 8 Hodge matrix $\mathbb{H}^{\tilde{0}2}$

2.4. Eigenvalues of the pressure matrix

The pressure matrix formed by $\tilde{\mathbb{E}}^{21}\mathbb{H}^{\tilde{1}1}\mathbb{E}^{10}$, is a singular matrix. To understand this singularity, the eigenvectors and eigenvalues are calculated numerically for the case of $N = 3$. As it was done numerically, the exact singularity was not present, however, the smallest eigenvalue was found to be $1.58 \cdot 10^{-15}$. The associated eigenvector can be assumed to approximate the basis of the kernel of the exact matrix. The found eigenvectors components were all equal, thus the kernel of the matrix is the span of a vector containing the same elements everywhere. This singularity in a physical sense represents the fact that in the incompressible Navier-Stokes equations there is no unique solution for the pressure, as the pressure can be shifted by a constant value everywhere and the equations are still satisfied.

2.5. Final discrete system

With all the ingredients such as the incidence and Hodge matrices introduced and set up, the final system is ready to solved. This final system is written from (1), (2) and (3) and it can be presented as

$$\frac{u^{n+1}-u^n}{\Delta t} + \text{ convective }^n + \mathbb{E}^{10}P^{n+1} + \frac{1}{Re}\mathbb{H}^{1,\tilde{1}}\widetilde{\mathbb{E}}^{10}\mathbb{H}^{\tilde{0}2}\left(\xi^n + \xi_{\text{prescr}}\right) = 0 \tag{21}$$

$$\mathbb{E}^{21}\mathbb{H}^{\tilde{1}1}u^{n+1} + u_{norm} = 0 \tag{22}$$

$$\xi^n = \mathbb{E}^{21}u^n\,, \tag{23}$$

where n represents the time step of the iteration. Thus, this system is solved implicitly. It is taken that the conservation of mass for time step $n+1$ is 0 as shown in (22) but for time step n, non-zero value is assumed in order to minimise error induced by accounting for the minor error that could blow up.

2.6. Post processing of data

To compare the resultant data to the reference data, the pressure in the domain has to be shifted to be consistent with the reference data, as the pressure solution is unique up to a constant. The choice made by Botella and Peyret in [2] is that pressure in the centre of the domain is 0. Furthermore, this pressure is the static pressure, while the numerical solver works with the total pressure of the flow given by

$$P = p + \frac{1}{2}||u||^2 \tag{24}$$

As the velocity is known, the static pressure can easily be calculated for the solution. To calculate the stream function, first, a relationship between the stream function and a known variable has to be found. As can be seen in Figure 1, the stream function defined on the primal points is related to the velocity flux through the primal edges by the incidence matrix $E^{\tilde{1}0}$, which corresponds to the perpendicular gradient. From this, a linear system can be formed.

$$\tilde{\mathbb{E}}^{10}\psi^{(0)} = \tilde{u}^{(1)} \tag{25}$$

As this system is not formed by a square matrix, a least square solver is used. The resulting streamfunction is only unique up to a constant. In order to compare the results, the value of $\psi^{(0)}$ is defined to be 0 on the stationary walls.

3. Results and validation

With the numerical solver setup, validation of its working was preformed for a lid-driven cavity case. This validation was performed against the results of a spectral method by Botella and Peyret [2].

3.1. Determination of convergence criteria

In the simulation, all walls were kept stationary except the top wall which was moving to the left with a speed of 1 m/s. The simulation was performed at 5 different resolutions. To determine the tolerance at which steady-state flow is assumed to be reached, the numerical simulation was run to a tolerance of 10^{-12} for $N = 31$ and the deviation of the velocity at the centre of the domain to the validation data was recorded for different reached tolerances. This is plotted in Figure 9 together with the computational cost needed for achieving a tolerance.

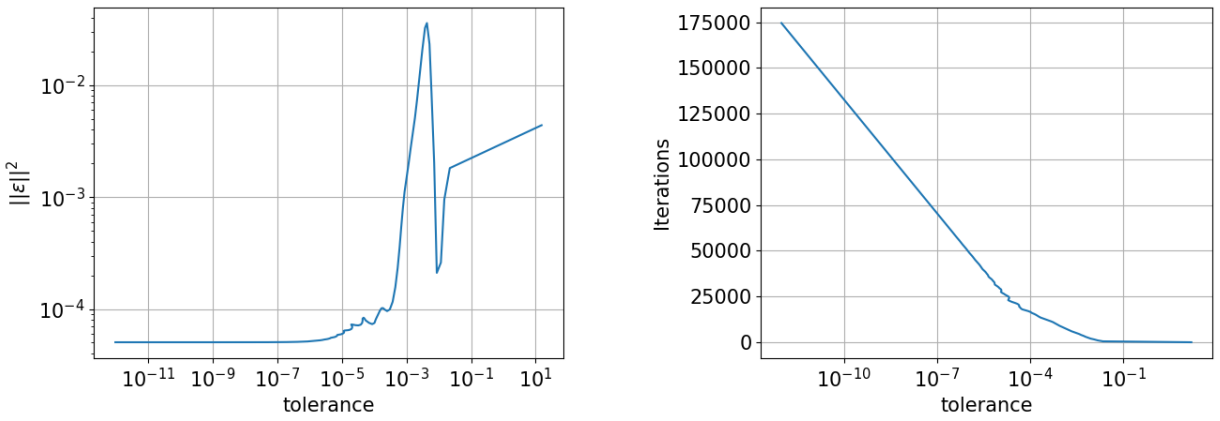

(a) Convergence of velocity at the center **(b) Number of iterations needed for reaching a tolerance**

Fig. 9 Convergence behaviour and cost of velocity in the center for N = 31

It can be seen that the accuracy of the solution does not decrease significantly for tolerances below 10^{-6}. The computational cost however still increases linearly to the *log* of the tolerance. From this it is chosen to run the simulation up to a tolerance of 10^{-6} for all further simulations. The largest stable timestep was chosen such that the Courant-Friedrichs-Lewy-Number (CFL-Number) was a maximum of 1, as well as the viscous diffusion term being stable as shown in (26). As this timestep is rather conservative, multiples of this timestep were tried. It was found that twice this timestep was stable for all attempted mesh resolutions.

$$\Delta t = 2 \cdot min\left(h_{min}, \frac{1}{2} Re h_{min}^2\right) \tag{26}$$

3.2. Comparison of the solution on the centerlines

To assess the accuracy of the solver, the velocity, pressure and vorticity were plotted on the horizontal and vertical centerline and compared to the results provided in [2]. The horizontal velocity through the vertical centerline and the vertical velocity through the horizontal centerline are shown in Figure 10. Furthermore, the pressure and vorticity are plotted along the centerlines and compared to Betella and Peyret [2]. The corresponding graphs are presented in Figure 11 and Figure 12 respectively.

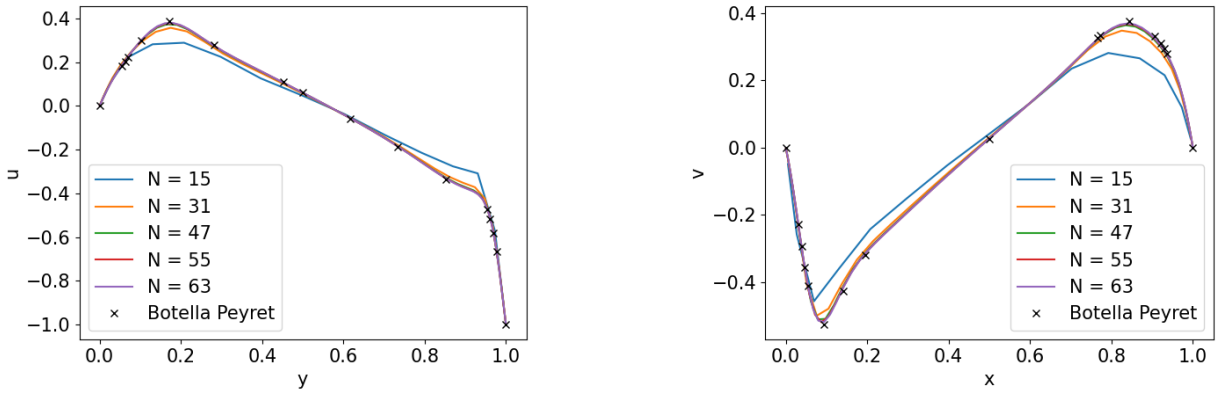

(a) Horizontal velocity through the vertical centerline **(b) Vertical velocity through the horizontal centerline**

Fig. 10 Comparison of velocity profiles through the centerlines against validation data

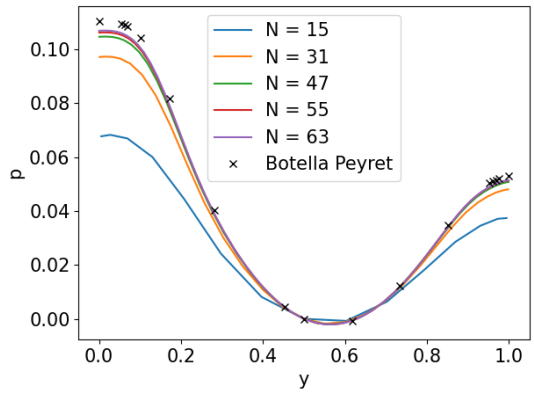

(a) Pressure along the vertical centerline

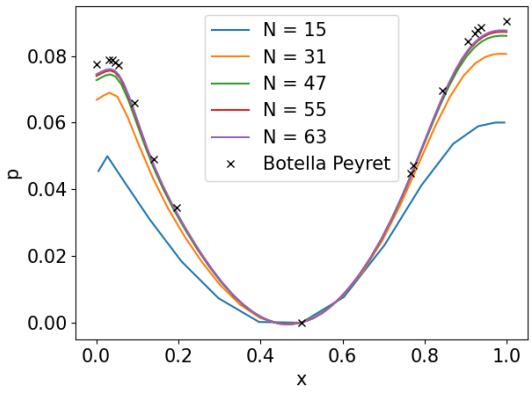

(b) Pressure along the horizontal centerline

Fig. 11 Comparison of pressure profiles through the centerlines against validation data

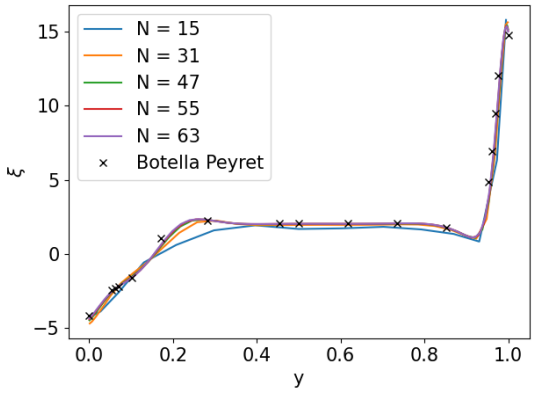

(a) Vorticity along the vertical centerline

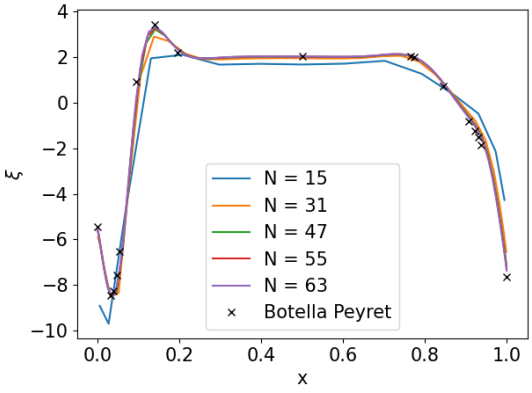

(b) Vorticity along the horizontal centerline

Fig. 12 Comparison of pressure profiles through the centerlines against validation data

From the figures, it can be seen that the general structure of the solution is replicated by our numerical method for $N \geq 47$. In order to quantitatively assess the performance of solver, the norm of the difference between our solution and the reference solution is calculated. This value is then normalized by the norm of the vector holding the reference values. This can be expressed for a quantity x by

$$\varepsilon_x = \frac{||x - x_{ref}||}{||x_{ref}||} . \tag{27}$$

The result from these calculations can be found Table 1 and Table 2.

Table 1 Error quantification on the vertical centerline

N	ε_u	ε_p	ε_ξ
15	0.10798	0.36733	0.26416
31	0.03503	0.11653	0.17911
47	0.01745	0.05185	0.13066
55	0.01261	0.03810	0.11306
63	0.00994	0.03266	0.09922

Table 2 Error quantification on the horizontal centerline

N	ε_u	ε_p	ε_ξ
15	0.16324	0.36804	0.25871
31	0.05083	0.11918	0.11500
47	0.02221	0.05353	0.07509
55	0.01649	0.03958	0.06690
63	0.01244	0.03408	0.05768

It can be seen that the total error for velocity on the horizontal and vertical centerlines are of the order of 1% for the finest mesh. For the pressure, it can be seen that the total error for the pressure in the cavity is of the order of 3-4%. This is significantly higher than for velocity. It can however be seen from the figures that this difference mostly originates from the inaccuracy at the boundary, which also displays a strong convergence behaviour. From all three properties, the vorticity displays the biggest error when compared to the velocity. As vorticity can, however, be calculated from velocity with the help of incidence matrices and Hodge matrices, this bigger error may have originated from the assumptions made when setting up the Hodge matrices. Another way to qualitatively evaluate the solver is by comparing the maximum and minimum values of velocity on the centerlines to reference data.

Table 3 Comparison of minimum and maximum values of velocity on the centerlines of the domain

Reference	N	u_{max}	v_{max}	v_{min}
Present	15	0.288906	0.281618	-0.457509
Present	31	0.357218	0.348175	-0.500378
Present	47	0.373142	0.364270	-0.511355
Present	55	0.376519	0.367684	-0.519710
Present	63	0.379753	0.369522	-0.519129
Ref [2]	48	0.3885271	0.3768991	-0.5270168
Ref [2]	160	0.3885698	0.3769447	-0.5270771

The produced data shows good agreement with the reference data. It is however to be noted that the velocity extrema are underpredicted when compared to results of [2]. This could be caused by dispersive numerical schemes. As the values of vorticity and velocity were assumed constant over the elements in the setup of Hodge matrices, such an assumption will smooth out small oscillations leading to the observed dispersed solution.

3.3. Qualitative Comparison of the flow field

A qualitative evaluation is performed, by comparing the vorticity, pressure and stream function contours of the method to [2]. The contour levels were chosen according to the level in [2] for comparison. The results are presented for 5 different mesh levels as well as for the validation solution in Figure 13, Figure 14 and Figure 15.

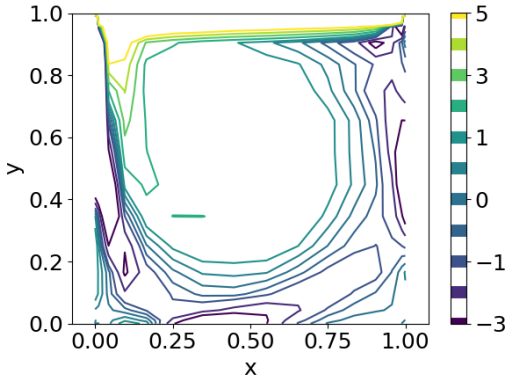

(a) N=15

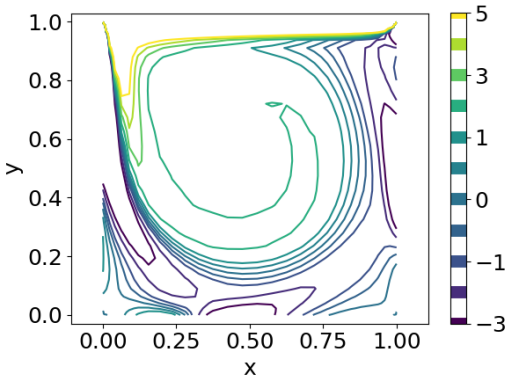

(b) N=31

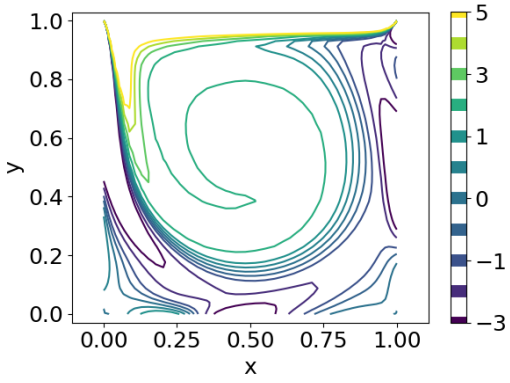

(c) N=47

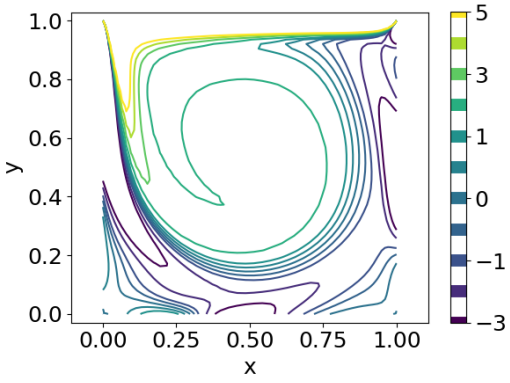

(d) N=55

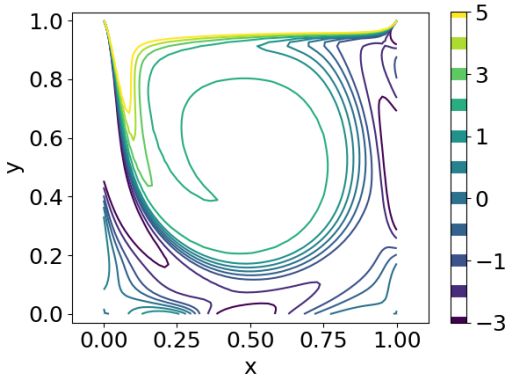

(e) N=63

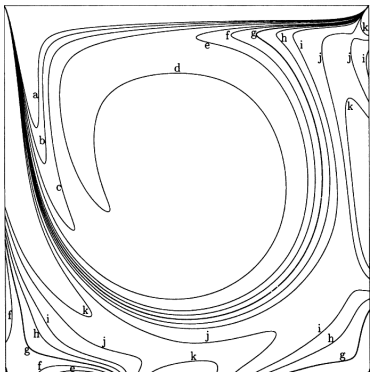

(f) Botella and Peyret [2]

Fig. 13 Comparison of isovorticity contours for different mesh resolutions against reference data

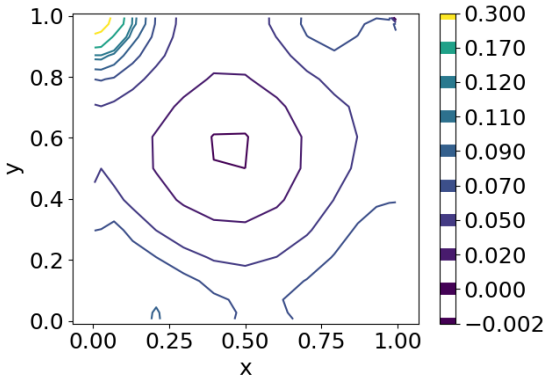

(a) N=15

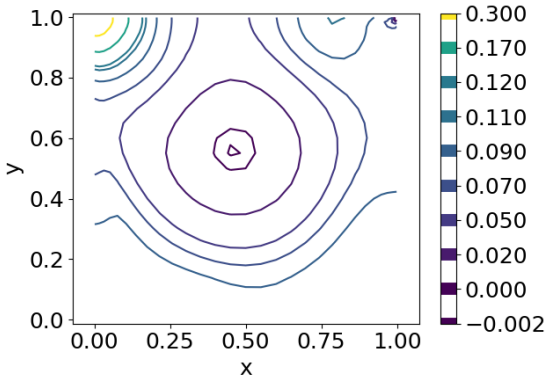

(b) N=31

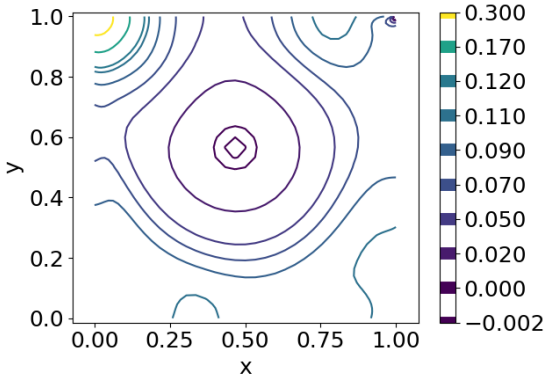

(c) N=47

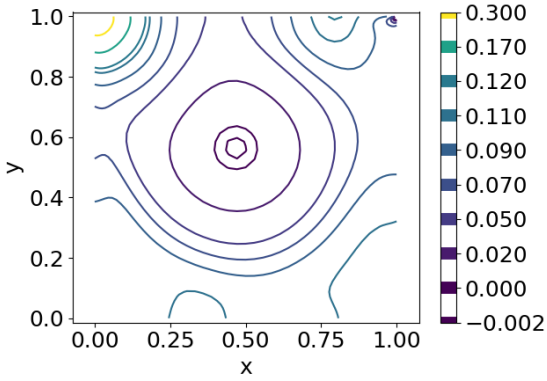

(d) N=55

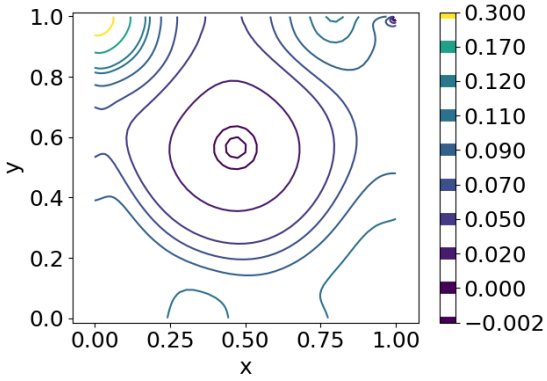

(e) N=63

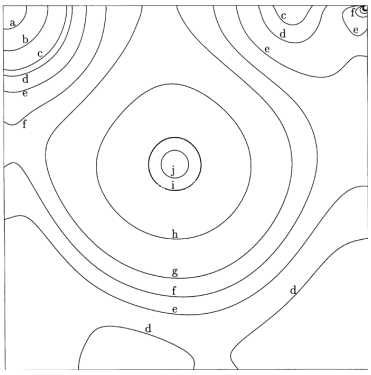

(f) Botella and Peyret [2]

Fig. 14 Comparison of isobaric contours for different mesh resolutions against reference data

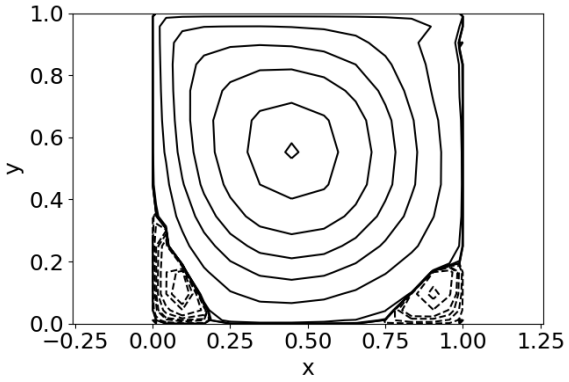

(a) N=15

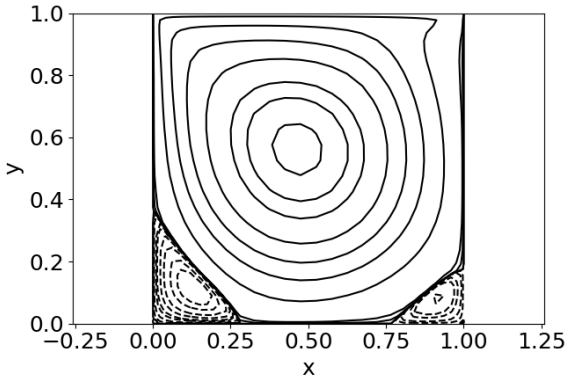

(b) N=31

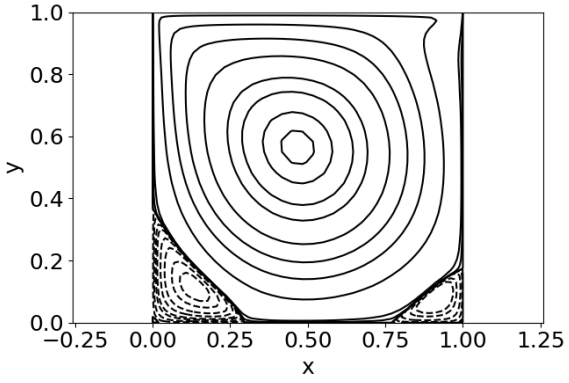

(c) N=47

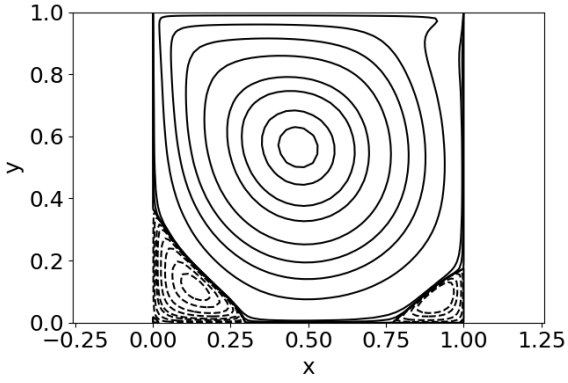

(d) N=55

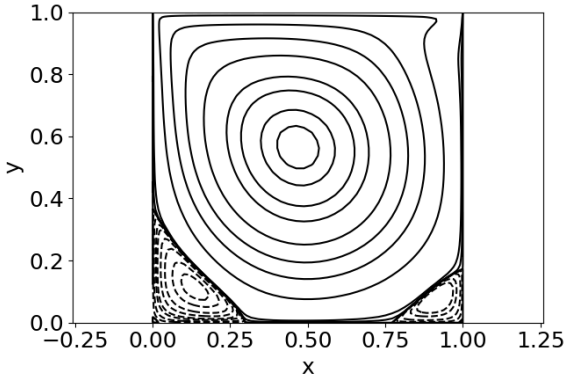

(e) N=63

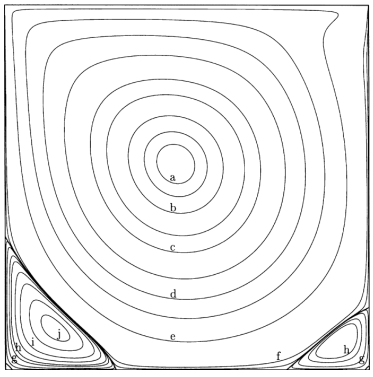

(f) Botella and Peyret [2]

Fig. 15 Comparison of stream function contours for different mesh resolutions against reference data

From these comparisons, it can be seen that the general structure of the flow is already captured at the lowest resolutions, however, more accurate contours are only produced at higher resolutions. When comparing the stream function it can be seen that the maximum value at the centre of the vortex is underpredicted when compared to the reference, this can again be caused by a dispersive numerical scheme, as noted before.

3.4. Dependence of vorticity to Reynolds number

In a further step, the dependence of total vorticity in the domain on the Reynolds number was analysed. For all Reynolds numbers, this value was found to be 1, thus no dependence on Reynolds number was found. This is consistent as the total vorticity depends on the boundary conditions of the domain as can be seen in (28). As the tangential velocity on the boundary is defined independent of Reynolds number, this value is constant over different Reynolds numbers.

$$\int_S \xi \, \mathrm{d}A = \int_S \nabla \times \mathbf{u} \, \mathrm{d}A = \int_{\partial S} \mathbf{u} \cdot \mathrm{d}\mathbf{l} \tag{28}$$

References

[1] Gerritsma, M., "AE4136: CFD II: Discretization techniques," , 2016.

[2] Botella, O., and Peyret, R., "Benchmark spectral results on the lid-driven cavity flow," *Computers and Fluids*, Vol. 27, No. 4, 1998, pp. 421–433. doi:10.1016/S0045-7930(98)00002-4.